

Research Article

A riverbank failure model: A case study for the segment of Tien River flowing through Sadec, Vietnam

Kim Tran Thi¹, Diem Phung Thi My¹, Huy Nguyen Dam Quoc², Tai Pham Anh^{3,4}, Phung Nguyen Ky¹, Bay Nguyen Thi^{3,4*}

¹ Ho Chi Minh City University of Natural resources and Environment, 236B Le Van Sy Street, Ward 1, Tan Binh District, Ho Chi Minh City; ttkim@hcmunre.edu.vn; diemptm@hcmunre.edu.vn; kyphungng@gmail.com

² Institute of Coastal and Offshore Engineering, Vietnam, 658 Vo Van Kiet, Ward 1, District 5, Ho Chi Minh City, Vietnam; damquochuy71@gmail.com

³ University of Technology Ho Chi Minh City, Vietnam, 268 Ly Thuong Kiet Street, Ward 14, District 10, Ho Chi Minh City; phamanhtai0410@gmail.com; ntbay@hcmut.edu.vn

⁴ Vietnam National University Ho Chi Minh City, Linh Trung Ward, Thu Duc District, Ho Chi Minh City, Vietnam; phamanhtai0410@gmail.com; ntbay@hcmut.edu.vn

*Correspondence: ntbay@hcmut.edu.vn; Tel.: +84–902698585

Received: 14 April 2023; Accepted: 31 May 2023; Published: 25 September 2023

Abstract: Riverbank erosion is a common occurrence in rivers worldwide, leading to significant impacts on shoreline protection and the lives of people residing in affected areas. Scientists, experts, and engineers have devoted considerable attention to study this phenomenon to better understand and predict the damage caused by riverbank failures. In the paper, we propose a mathematical model that combines bottom erosion and riverbank failure mechanisms. The model incorporates high-performance GPUs (Graphics Processing Units) to enhance its computational efficiency and capability. It utilizes a set of equations, such as the Reynolds equations, sediment transport equations, and bed load continuity equation, to simulate the dynamics of flow, sediment transport, and changes in the riverbed. Additionally, the model incorporates the calculation of riverbank failure using the rotational failure mechanism and determines the factor of safety (FS) to assess the stability of riverbanks and the bank failure (BW). If the FS value is less than 1, it indicates that the bank is prone to failure, and such instances are recorded. To evaluate the model's reliability, a case study is conducted on a specific segment of the Tien River in Sa Dec City, Dong Thap Province. This model serves as a crucial tool for socioeconomic planning and implementing effective measures to prevent and mitigate the impacts of riverbank failure in the local area.

Keywords: Bed erosion; Factor of safety; Rotational failure; River instability; Riverbank failure.

1. Introduction

The morphological development of river systems is the most common issue that occurs in all rivers around the world. There are numerous studies investigating the evolution of morphology in river systems that are disrupted by natural and artificial factors such as dam construction, channel modifications, land use changes, volcanic eruptions, etc. [1–9]. To adequately describe and predict the geomorphic responses in a fluvial system, four components of channel change should be considered: direction, magnitude, time rate, and

spatial extent. Direction refers to the direction of change, such as erosion or deposition, while magnitude relates to the size or scale of the change. Time rate refers to the speed at which changes occur, and spatial extent pertains to the area over which changes occur [10–11]. These four components are interdependent and influence each other in complex ways. For instance, the direction of change can affect the spatial extent, while the magnitude of change can impact the time rate. Therefore, it is essential to consider all four components together to develop a comprehensive understanding of channel change in a fluvial system. This understanding can then be used to make accurate predictions about future changes, such as the effects of environmental or human-induced disturbances [9–10, 12–14].

The equilibrium concept or relaxed state associated with the tendency for responses to disturbance explains the complexity of intrinsic and extrinsic mechanisms in the fluvial systems and their response [12, 15–16]. Therefore, this precludes the development of empirical or experimental approaches coupled with physical-mathematical modeling, which are expected to simulate and predict the morphological responses of fluvial systems to intrinsic and extrinsic disturbances [17].

For the 2D hydrodynamic, sediment transport, and river morphology models, several widely applied and developed models exist worldwide. Some notable examples include:

MIKE model: Developed by DHI in Denmark, this integrated model offers various tools and performs well in addressing river erosion problems [18]. Delft model (DELFT2D): Developed by Deltares in the Netherlands, this model is widely used for hydrodynamic simulations [19]. TELEMAC model: Initially developed in 1987 by Electricité de France (EDF) in collaboration with multiple research organizations, this model is widely used for hydraulic simulations [20]. SMS (Surface Water Modeling System): Developed by the Waterways Experiment Station (WES) and the Army Corps of Engineers in the United States, this model combines hydrodynamics and sediment transport simulations [21]. CCHE2D model: Developed by the author [22], this model has the capability to simulate two-dimensional hydrodynamic characteristics. SUTRENCH-2D model: Developed by the author [23], this model simulates sediment transport and bed variations under combined flow conditions. FLUVIAL 12 model: Developed by the author [24], this model is used for river flow and sediment transport simulations. Besides the mentioned models, there are also other software packages available, such as USTARS, developed by the author [25], etc. In addition, there are also several widely used software packages developed and applied in Vietnam, such as: F28 model: Developed by Le Song Giang, this is a 2D model (similar to MIKE FLOOD) that combines 1D river flow and 2D floodplain flow. It allows for the simulation of flow dynamics in both river channels and floodplains [26]; TREM model: Developed by the author [27], based on the corresponding 2D flow model by Nagata from Kyoto University, Japan. This model simulates 2D river channel deformation in a non-orthogonal curvilinear coordinate system, allowing for the determination of velocity distribution and riverbed changes in both longitudinal and transverse directions; HYDIST-GPUs model: Developed by the author [28], HYDIST-GPUs is a model capable of simulating 2D flow, sediment transport, and river morphology changes, etc.

These existing models are based on the principles of dynamic equations and continuity equations integrated in the vertical direction. However, there are still limitations in the integration of bank failure calculations within the existing software packages.

A recent approach to studying riverbank failure is using a simple dynamic risk model with time-varying covariates to develop an early warning model for bank failures, then testing the out-of-sample predictive accuracy of this model against a simpler model - the periodic probit model, such as used by US banking regulatory agencies [29]. To understand the mechanism of sudden riverbank failure, previous studies have attempted to integrate soil erosion processes and changes in riverbank geometry into the analysis of riverbank stability [30–31].

The author [32] developed a mathematical model to calculate simple bank erosion, which is integrated into the 2D Saint-Venant-Exner morphodynamic model (in the TELEMAC 2D model). The computational grid is built on a structured triangular grid and a finite element algorithm. The slope of each element in the grid is compared with the slope of the bank material. Elements with too steep slopes are determined so that the lost mass above the axis equals the increased mass below, thus ensuring mass balance. The model performance is evaluated using data from smoke tube experiments in the laboratory and the scale model of the Old Rhine.

Furthermore, the author [33] conducted a numerical modeling and field monitoring integrated study at six specific research sites in the United Kingdom. In this study, stability analysis was based on the safety factor. Pore water pressure data was calculated at each time step in the simulation and combined with observed geotechnical data to adjust the mechanical effects of roots and vegetation cover. Similarly, the author [34] conducted a stability analysis for the waste dump slope of the WCL Makardhokara-2 open cast mine in Umred, Nagpur district, Maharashtra, India. In this study, slope stability analysis was performed using seven specific finite slope stability methods including Morgenstern's method, Spencer's method, Sarma's method, Bishop's method, Janbu's method, and the conventional method using GeoSlope software for the waste dump slope in the Makardhokara area.

In this study, we propose a simple mathematical model that combines hydrodynamic, sediment transport, river morphology effects and stability analysis of riverbanks. The HYDIST-GPUs model incorporates high-performance GPUs (Graphics Processing Units) to enhance its computational capabilities. It utilizes the Reynolds equations, sediment transport equations, and bed load continuity equation to simulate various aspects of the river system, including flow behavior, sediment transport processes, and changes in the riverbed. By leveraging the power of GPUs, the model can achieve faster and more efficient calculations, enabling more detailed and accurate simulations of the river dynamics. These equations are solved numerically to determine the stability tendency and track the behavior of suspended or deposited materials [28]. Additionally, cross-sections are extracted using the rotational failure mechanism and the factor of safety (FS) to assess the stability of riverbanks and the likelihood of failure (RF module). To validate the model's accuracy, a case study is conducted on a specific segment of the Hau River in Chau Phu district, An Giang Province. The results obtained from this case study demonstrate a remarkable agreement between the calculations derived from our model and the observed measurements, indicating the model's capability to accurately predict the stability and sediment dynamics of the riverbanks.

2. Materials and Methods

2.1. Study area

The study area is the section of the Tien River passing through Sa Dec city, Dong Thap province, as illustrated in Figure 1. The section of the Tien River that flows through Sa Dec city is a typical example of a meandering river, where bank erosion has been occurring continuously over the past few decades at a rate of up to 30 meters per year, and sometimes reaching 50 meters per year [6]. The total length of the eroded bank is up to 10 kilometers and it has eroded more than 3 kilometers into the land. The bank erosion has destroyed many important structures in Dong Thap province, including roads, hospitals, schools, and government offices [6].

2.2. Material

The bathymetry data used in the model is derived from the measurements conducted in 2017 and water level (Z), discharge (Q) and suspended sediment (C) at ST5 (from June 6,

2018, to June 13, 2018) (Figure 1) as part of the project titled “Development of bank erosion numerical model basing on HPC in connection with hydraulic model and to apply for some river reaches of the Mekong River” under grant No. NĐT.28.KR/17.

The hourly water level measurements (Z) at Cao Lanh station and discharge measurements (Q) at My Thuan station from 00:00 on May 15, 2014, to 23:00 on December 31, 2017, were collected from the Southern Region Hydro-Meteorological Centre as boundary conditions for the model.

The hourly suspended sediment concentration (C) at the boundaries is extracted from the Mike 11 model of the project titled “Development of bank erosion numerical model basing on HPC in connection with hydraulic model and to apply for some river reaches of the Mekong River” under grant No. NĐT.28.KR/17.

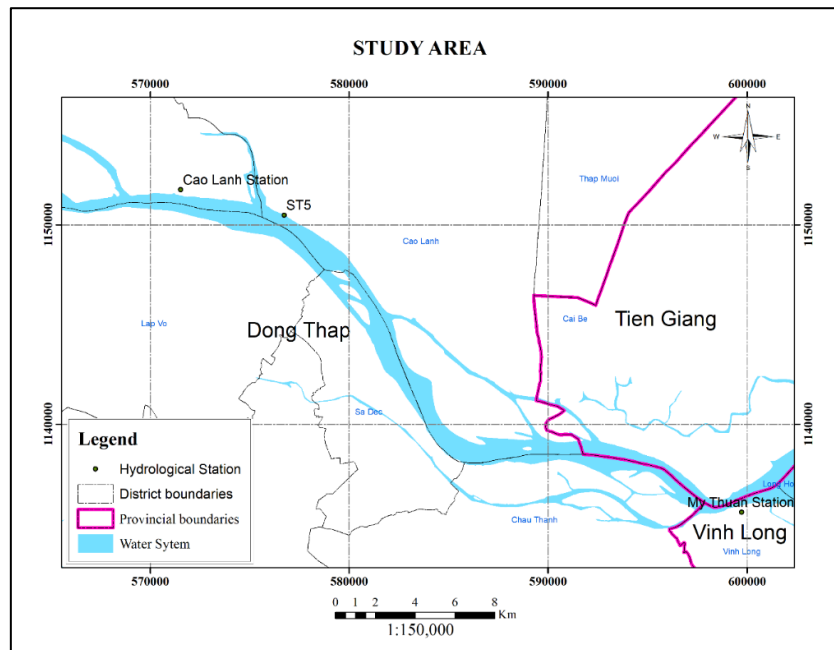


Figure 1. The section of the Tien River passes through Sa Dec city, Dong Thap province.

2.3. Method

A simple mathematical model that combines hydrodynamic, sediment transport, river morphology effects, and stability analysis of riverbanks is the HYDIST-GPUs model, which includes the integration of the RF module. The HYDIST-GPUs model is based on a set of equations, including the Reynolds equations, sediment transport equations, and bed load continuity equation [28].

2.3.1. Governing equations of the HYDIST-GPUs model

Reynolds equations:

$$\frac{\partial u}{\partial t} + u \frac{\partial u}{\partial x} + v \frac{\partial u}{\partial y} - fv = -g \frac{\partial \zeta}{\partial x} + \frac{\tau_{Sx,wind} - \tau_{Sx,w}}{\rho(h + \zeta)} - \frac{\tau_{bx}}{\rho(h + \zeta)} + A\nabla^2 \bar{u} \quad (1)$$

$$\frac{\partial v}{\partial t} + u \frac{\partial v}{\partial x} + v \frac{\partial v}{\partial y} + fu = -g \frac{\partial \zeta}{\partial y} + \frac{\tau_{Sy,wind} - \tau_{Sy,w}}{\rho(h + \zeta)} - \frac{\tau_{by}}{\rho(h + \zeta)} + A\nabla^2 \bar{v} \quad (2)$$

$$\frac{\partial \zeta}{\partial t} + \frac{\partial [(h + \zeta)u]}{\partial x} + \frac{\partial [(h + \zeta)v]}{\partial y} = 0 \quad (3)$$

where the “zero level” is set at the still water surface (Figure 2); u, v are depth-averaged horizontal velocity components in x, y direction respectively; h is static depth from the still

water surface to the bed and ζ is the water level. To simplify the simulation process for the river, we neglect the Coriolis force f and wind stress ($\tau_{Sx,wind}, \tau_{Sy,wind}$) as well as wave stress ($\tau_{Sx,w}, \tau_{Sy,w}$) in both x, y directions [28].

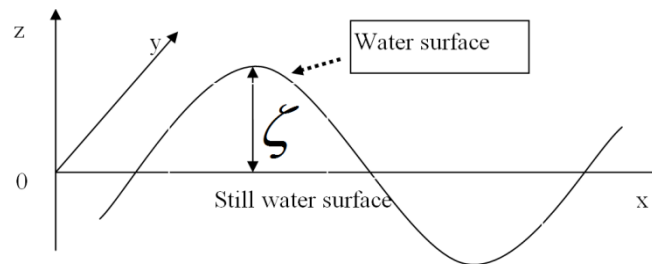


Figure 2. Initial static level.

Sediment transport equations

Due to two types of suspension: bed load and suspended load, we define the bed load having a thickness of a and at the elevation of z , hence: $-h < z < -h + a$.

The suspended load is defined in the water and at the elevation of z , where $-h + a < z < \zeta$. The minimum experimental value of a can be $0.01 H$ [35]. So, the depth-averaged mass balance equation for suspended sediment will be described as follows:

$$\frac{\partial C}{\partial t} + \gamma_v \left(u \frac{\partial C}{\partial x} + v \frac{\partial C}{\partial y} \right) = \frac{1}{H} \frac{\partial}{\partial x} \left(HK_x \frac{\partial C}{\partial x} \right) + \frac{1}{H} \frac{\partial}{\partial y} \left(HK_y \frac{\partial C}{\partial y} \right) + \frac{S}{H} \quad (4)$$

where H is the relative depth (m), and defined by static depth h and fluctuation ζ (Figure 2), $H = h + \zeta$. The quantity S describes deposition or erosion of grain ($\text{kg/m}^2\text{s}$), and can be calculated by Van Rijn’s empirical equations [35].

The bed load continuity equation can be described as the following equation.

$$\frac{\partial h}{\partial t} = \frac{1}{1 - \epsilon_p} \left[S + \frac{\partial}{\partial x} \left(HK_x \frac{\partial C}{\partial x} \right) + \frac{\partial}{\partial y} \left(HK_y \frac{\partial C}{\partial y} \right) + \frac{\partial q_{bx}}{\partial x} + \frac{\partial q_{by}}{\partial y} \right] \quad (5)$$

where q_{bx}, q_{by} , standing for the rate of bed load transport in x, y directions ($\text{m}^2/\text{s}/\text{m}$), can be determined by experimental formula [35].

$$q_b = 0.053((S - 1)g)^{0.5} d_m^{1.5} T^{2.1} D_*^{-0.3} \frac{(u, v)}{\sqrt{u^2 + v^2}} \quad (6)$$

where $q_b = (q_{bx}, q_{by})$.

3.2.2. Riverbank failure mechanism and factor of safety – RF module

The riverbank failure will be calculated on the rotational failure [36–37]. The mechanism of sliding motion illustrated in Figure 3 is explained by the fact that bank materials move to two directions: downward and outward along circular slip surface, and this is common on cohesive banks with slopes less than 60° . After failure, the upper slope of the slipped block is typically tilted inward toward the bank. Rotational failures are commonly a result of scour at the base of the bank and/or high pore-water pressure within the bank material. Normally, they will occur during rapid drawdown following high flow events.

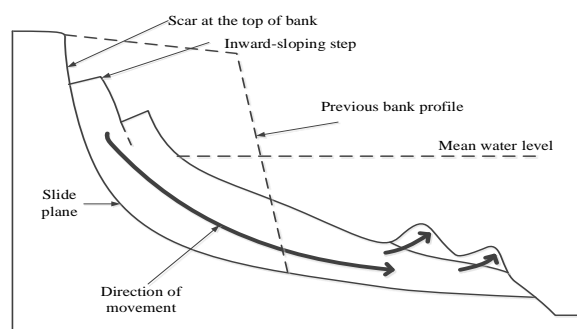


Figure 3. Mechanism of rotational failure (from Environment Agency [38]).

The critical threshold of riverbank stability can be quantified by the FS. An FS < 1 is indicative of instability and the bank failure. If FS = 1, these forces are exactly balanced. As FS increases beyond unity, the slope becomes more stable.

To determine FS, it is necessary to calculate the total forces and total moment forces acting on the sliding mass in both horizontal and vertical directions. The components used to determine the forces and moment forces include known components and unknown components. However, there are fewer known components compared to unknown components. In the model, the following assumptions are accepted:

Neglecting the interaction forces between slices when separating them into individual slices: The model uses two methods: (i) the Fellenius method (neglecting the interaction forces between slices $E = X = 0$) [39]; (ii) the Bishop method (neglecting the vertical component $X = 0$) [40].

The interaction path-locus of the point of application of the interaction force: The model uses the general Janbu method and the simplified Janbu method [41].

The inclination angle of the interaction force: The model uses the Spencer and the General Limit Equilibrium (GLE) methods [42].

These assumptions are made to simplify the analysis and calculation process. While they may introduce some limitations, they allow for the estimation of the factor of safety and provide valuable insights into the stability of the analyzed slope.

The FS includes two independent factor of safety equations; one with respect to moment equilibrium and the other with respect to horizontal force equilibrium.

When only moment equilibrium (F_m) is satisfied, the factor of safety equation is:

$$F_m = \frac{\sum(c'\beta R + (N - u\beta)R \tan\phi)}{\sum W_x - \sum Nf + \sum kW_e \pm \sum Dd \pm \sum Aa} \quad (7)$$

The factor of safety equation with respect to horizontal force equilibrium (F_f) is:

$$F_f = \frac{\sum(c'\beta \cos\alpha + (N - u\beta) \tan\phi \cos\alpha)}{\sum N \sin\alpha + \sum kW_e - \sum D \cos\omega \pm \sum A} \quad (8)$$

where F_m is the moment equilibrium factor of safety; F_f is the force equilibrium factor of safety; W is the slice weight with width b and height h [kN]; N is the slice base normal force [kN]; D is the concentrated point load [kN]; kW is the horizontal seismic load acting through the center of gravity of each slide [kN]; R is the radius of the circular slide (or the arm of the shear force moves for any shape of the slide) [m]; A is the resultant force of water pressure acting on the bank [kN]; f is the distance from center of rotation to direction of normal force N [m]; x is the horizontal distance from center of gravity of each slide to center of rotation or center of moment [m]; e is the vertical distance from the center of each slide to the center of rotation or center of moment [m]; d is the perpendicular distance from load line to center of rotation or center of moment [m]; a is the perpendicular distance from the external water force to the center of rotation or center of moment [m]; ω is the angle of inclination of the force direction relative to the horizontal (determined in the same direction); α is the angle between the tangent at the base and the horizontal [degrees]. Sign convention: when the slip angle is in the same direction as the overall slide of the figure, α is positive and vice versa; ϕ is the effective angle of friction [degree]; u is the pore-water pressure [kPa]; c' is the effective cohesion [kPa]; β is the length of the sliding arc of the earth column [m].

The normal force at the base of the soil column is determined by summing the vertical forces acting on each soil column. To do this, we need to know the weight forces of each soil column ((9), as well as the other vertical forces acting on them.

$$N = \frac{W + (X_R - X_L) - \frac{c'\beta \sin\alpha + u\beta \sin\alpha \tan\phi}{F} + D \sin\omega}{\cos\alpha + \frac{\sin\alpha \tan\phi}{F}} \quad (9)$$

where: In the moment factor of safety equation, F is equal to F_m when N is substituted, indicating the moment resistance. On the other hand, in the force factor of safety equation, F is equal to F_f when N is substituted, representing the force resistance.

3.2.3. Simulation process

The integration of the riverbank failure module with the HYDIST-GPUs model, referred to as HYDIST-GPUs-RF, involves a sequence of steps in the simulation process. The steps are outlined as follows:

a) Discretization of the riverbank section

The section of the riverbank where there is a risk of erosion (simulated from the model) will be discretized into smaller segments by cross-sectional perpendicular to the riverbank. For each cross-section, the model will calculate the safety factor FS to identify the segments of the bank that are prone to erosion. Figure 4 illustrates the process of discretizing the riverbank section for the purpose of simulating bank erosion.

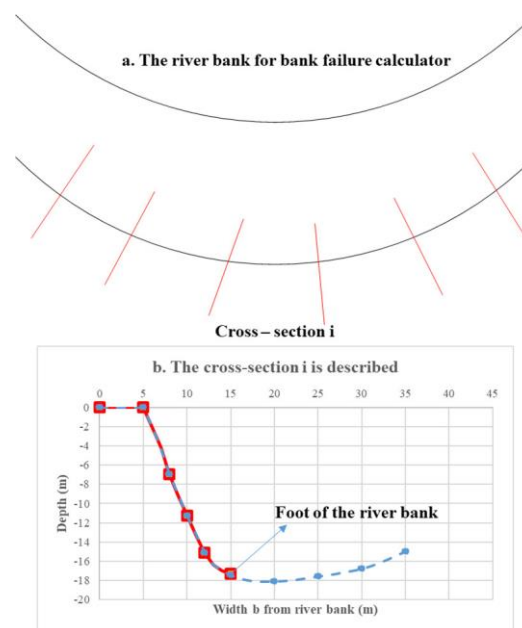


Figure 4. The process of discretizing the riverbank section for the purpose of simulating bank erosion.

The density of the cross-sections along the riverbank segment depends on the level of erosion risk, and in cases where there is low risk of erosion, the cross-sections will be spaced further apart. After calculating the safety factor of each cross-section, the degree of erosion will be calculated to determine the extent of bank collapse at that cross-section. The degree of erosion at any location between two cross-sections in the calculation area will be interpolated between the two cross-sections (using a linear interpolation method in the model).

b) Simulating the bank failure

After calculating the safety factor FS for each cross-section, if $FS \geq FS_{critical}$, then the bank slope at that cross-section is stable (not eroding), but if $FS < FS_{critical}$, then the bank slope at that cross-section is unstable and will erode. At this point, the direction of the bank slope will collapse inward with a width of BW . The value of BW (predicted width of bank collapse) at the i -th cross-section is compared with Δ ($\Delta = \sqrt{(\Delta x)^2 + (\Delta y)^2}$) to update the grid cell adjacent to the bank position at cross-section i , if $BW < \Delta$, then the characteristics of the bank cell are still preserved, and the hydraulic-erosion model continues to use the old topography for calculations until $BW \geq \Delta$. At this point, the bank cell will collapse and be converted into a fluid cell in the hydrodynamic flow problem. The comparison between BW and Δ is detailed in Table 1.

Table 1. Cases in which the bank plots are collapsed in the vertical direction i.

Cases	The number of cell–bank subsidence
$0 < BW < \Delta$	No falling
$\Delta \leq BW < 2\Delta$	1 cell
$2\Delta \leq BW < 3\Delta$	2 cells
$3\Delta \leq BW < 4\Delta$	
...	These cases are the same as above

For the positions of the bank cells located between two calculated cross sections i and $i+1$, the model also examines similarly to determine whether to convert those cells into liquefied cells or keep them as they are using the method above, with BW at each position determined by linear interpolation from the BW of cross sections i and $i+1$.

c) Bathymetry update

The section of land that has collapsed will slide down to the foot of the bank, causing changes in the depth values at this location (the top of the bank, the slope of the bank, and the foot of the bank). These changes need to be calculated to update the depth map for the next calculation of the dynamic hydraulics and sedimentation problem. The bank cells and slope cells will have a decreased bed elevation (increased depth). At the foot of the bank, sediment will be deposited, causing the bed elevation to increase (decreased depth). The extent of the bed elevation changes for each cell is calculated such that the volume of soil loss is equal to the volume of sediment deposited at the foot of the bank. Choose a cross-sectional view to explain this calculation. The cross-sectional view has been discretized into grid cells with the same size as the flow field discretization. Figure 5 depicts a cross-sectional view of a riverbank after discretization, with grid cells of size Δx .

The simulation results will give the parameters of the sliding arc radius and the center position O , from which the starting and ending points of the sliding arc can be determined to find the positions of the grid cells that need to be updated for the bottom topography (such as cells 2 to 6 in Figure 5).

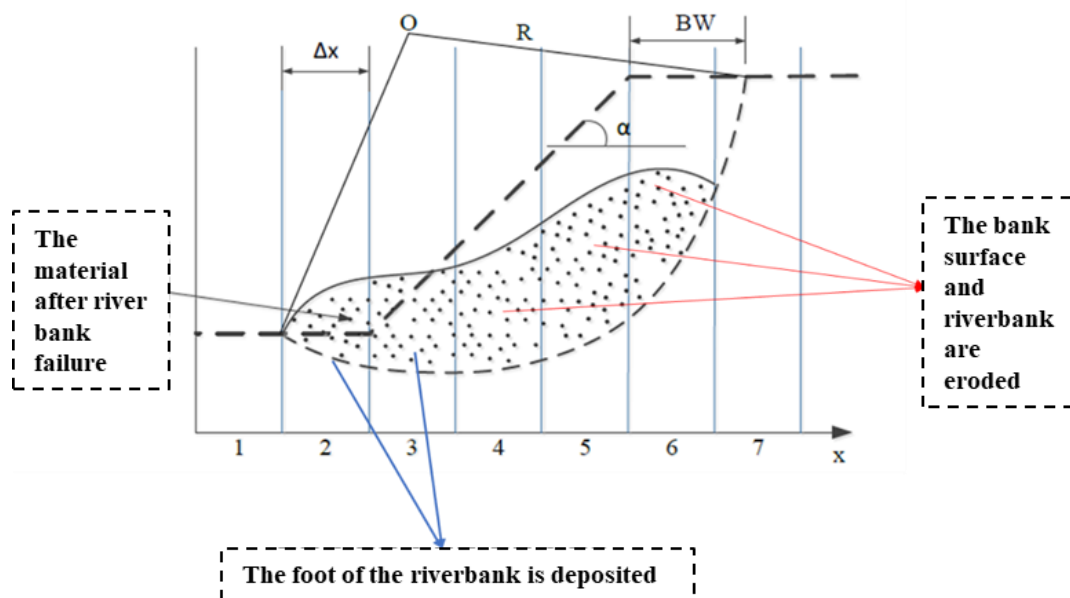


Figure 5. Riverbank cross-section before and after subsidence.

d) F_s safety factor

The general calculation scheme for bank erosion in the HYDIST-GPUs-RF model is presented in detail in Figure 6a, in which the steps for the safety factor in the bank erosion model are specifically presented in Figure 6b. When $F_m = F_f$, the factor of safety is calculated

as $FS = F_m$ or F_f . The sequence for calculating the safety factor F_s will be programmed using Python (suitable for GPUs) as the RF module to perform automatic calculations [28]. Then, the RF module will be integrated with the HYDIST-GPUs model to calculate the hydrodynamic process.

The diagram below illustrates the calculation process using two methods, Sarma and GLE. It is easy to see that the only difference between the two methods is the formula for the relationship between shear force (X) and normal force (E). Shear force and normal force at each cross-section on both sides will be distinguished by the symbols $X_L, X_R, E_L,$ and E_R .

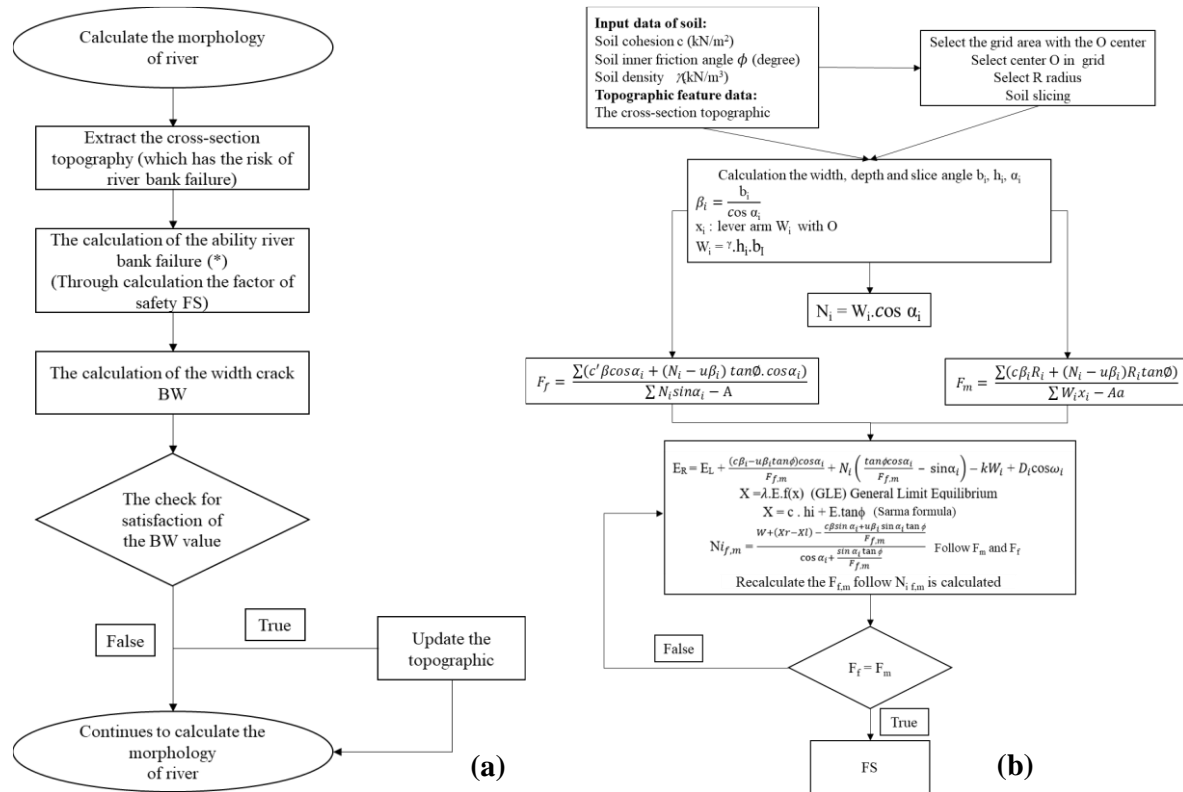


Figure 6. (a) HYDIST-GPUs-RF scheme; (b) FS scheme (*).

3. Results

3.1. Theory solution

The simplest form of the Ordinary factor of safety equation in the absence of any pore-water pressures for a circular slip surface is:

$$FS = \frac{\sum [c\beta + N \tan \phi]}{\sum w \sin \alpha} = \frac{\sum S_{resistance}}{\sum S_{mobilized}} \tag{10}$$

where c is the cohesion; N is the base normal ($W \cos \alpha$).

The ordinary factor of safety can be fairly easily computed using a spreadsheet. Using a spreadsheet is of course not necessary when you have HYDIST-GPUs-RF, but doing a simple manual analysis periodically is a useful learning exercise.

Consider the simple problem in Figure 7. There are 14 slices numbered from left to right. The cohesive strength is 5 kPa and the soil friction angle ϕ is 20 degrees.

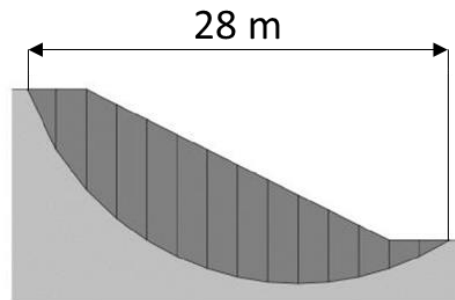


Figure 7. Case for hand-calculations.

Table 2 illustrates how the ordinary factor of safety can be easily calculated. The most difficult part is specifying the slice dimensions.

Table 2. The ordinary factor of safety.

Slice #	Width (m)	Mid-height (m)	Weight (kN)	Alpha (degrees)	β (m)
1	2	2.3	86.9	64.7	4.42
2	2	5.4	217.8	52.9	3.32
3	2	7.2	287	43.7	2.77
4	2	7.8	313.2	35.8	2.46
5	2	8.1	323.3	28.5	2.28
6	2	8	320.9	21.8	2.15
7	2	7.7	307.7	15.4	2.07
8	2	7.1	285.1	9.2	2.03
9	2	6.3	253.7	3	2
10	2	5.3	213.7	-3	2
11	2	4.1	165.1	-9.2	2.03
12	2	2.7	107.7	-15.4	2.07
13	2	1.5	60.9	-21.8	2.15
14	2	0.6	23.3	-28.5	2.28

The factor of safety can be computed to be:

$$FS = \frac{\sum [c\beta + N \tan\phi]}{\sum w \sin\alpha} = \frac{1116.75}{947.93} = 1.18 \tag{11}$$

HYDIST-GPUs-RF gives the same factor of safety as shown in Figure 8.

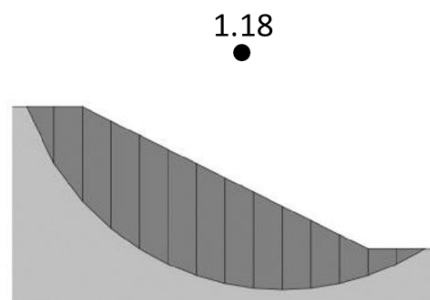


Figure 8. HYDIST-GPUs-RF computed ordinary factor of safety.

3.2. A case study for riverbank stability and riverbed erosion of Tien River (flowing Sa Dec city)

The occurrence of river bank erosion in Sa Dec has had severe consequences on bank protection structures and the lives of the local population. The erosion of riverbanks has compromised the effectiveness of protective measures, such as levees, revetments, or other bank defenses, that are crucial for safeguarding the area against the erosive forces of the river [43–44]. This erosion has resulted in the loss of land, damage to infrastructure, and potential threats to residential areas and livelihoods. The local community is directly affected by the negative impacts, including increased vulnerability to flooding, loss of agricultural land, and potential displacement of residents. Addressing and mitigating the impacts of river bank erosion in Sa Dec is of utmost importance to protect both the physical infrastructure and the well-being of the people living in the area.

In 2013, to prevent bank erosion, protect and stabilize the living environment for local residents, as well as contribute to the socio-economic development of the region, the provincial People's Committee built a system of revetments consisting of 7 sections, stretching about 4.5 kilometers from Cai Doi stream to Ong Tuan stream. The sedimentation and erosion processes in this area are relatively balanced. The concave bank on the right of the Tien River belongs to Ward 10 in Sa Dec city and An Hiep commune in Chau Thanh district, where bank erosion has been particularly strong. Although a system of revetments had been constructed in Ward 10 - Sa Dec, the distance between the revetments was not reasonable, so bank erosion still occurred at the foot of the revetments and in the areas between them. In March 2015, a serious bank erosion incident occurred at revetment section 7, causing many households to be urgently evacuated. Moreover, due to limited funding, only a section of the revetment system was constructed, while bank erosion in the area behind the revetment system in An Hiep commune - Chau Thanh district continues to occur continuously.

3.2.1. Mesh in HYDIST-GPUs

The research area is the section of the Tien River passing through Sa Dec city, divided into a grid of 484 rows and 629 columns, with a spacing of $dx = dy = 20$ m (Figure 9).

Number of rows = 484; Number of columns = 629; Total number of grid elements is $304,436 = 484 \times 629$; Maximum depth of the grid is $h = 40.96$ m.

Spatial step of the grid in the x-direction is $\Delta x = 20$ m, in the y-direction is $\Delta y = 20$ m, and the time step is $\Delta t = 2$ s.

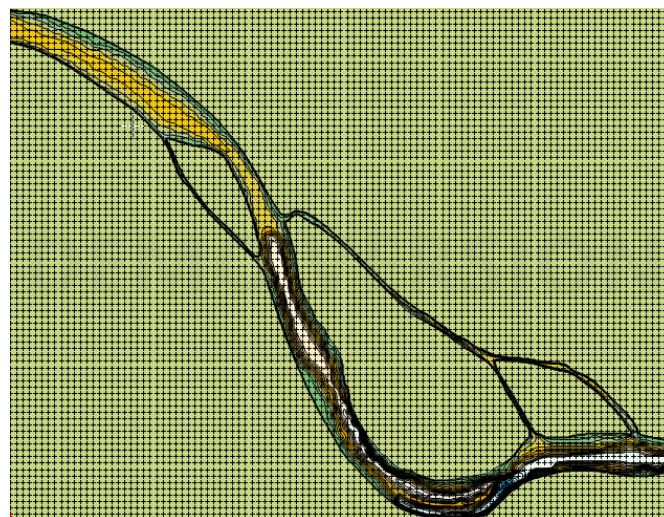


Figure 9. The depth map of the Tien River flowing Sa Dec with a 20-meter spacing.

3.2.2. Initial conditions and boundaries

For hydraulic model:

(1) Initial conditions: In the model, if we start the calculation from $t_0 = 0$, the hydraulic problem is initialized with a steady-state condition throughout the domain. In the case where the problem is continued from a specific time $t = t_1$, the initial conditions will be the velocity fields $u, v(x, y)$ at time t_1 across the entire computational domain.

(2) Boundary conditions:

Open boundaries: The first open boundary (B1) is determined by the measured water level value Z at the Cao Lanh station, which is shifted 8 hours ahead in the downstream direction.

The second open boundary (B2) is determined by the measured discharge value Q at the My Thuan station.

Both open boundaries are considered from 00:00 on May 15, 2014, to 23:00 on December 31, 2017.

Land boundaries: $u_n = 0$.

For sediment transport model:

(1) Initial conditions:

In the model, if the calculation starts from $t_0 = 0$, the sediment transport problem is initialized with a constant background concentration. In the case where the problem is continued from a specific time $t = t_1$, the initial condition will be the sediment concentration $C(x, y)$ at time t_1 throughout the computational domain.

(2) Boundary conditions:

Open boundaries: The suspended sediment concentration (C) at the boundaries is extracted from the Mike 11 model. However, the right boundary of the model does not utilize the characteristics of suspended sediment because this is where the water flows out of the computational domain. At this boundary, the model has used the method of characteristic lines to track the deposition of suspended sediment along the outflow. Both open boundaries are calculated from 15:00 on May 15, 2014, to 19:00 on December 31, 2014.

Land boundaries: $\frac{\partial C}{\partial n} = 0$, the variable “n” represents the normal direction perpendicular to the bank.

3.2.3. Calibration and validation

Calibration and validation of the hydraulic model

The results of discharge and water level calculations from the model at My Thuan in June 2014 compared to the accurately measured values are quite good. The NSE and R^2 values for water level calibration are high (0.98 and 0.96), indicating a good fit. Similarly, the NSE and R^2 values for discharge calibration are 0.97 and 0.93, respectively, indicating a good fit as well. It should be emphasized that the Sa Dec section, from the upper to lower reach, is a relatively

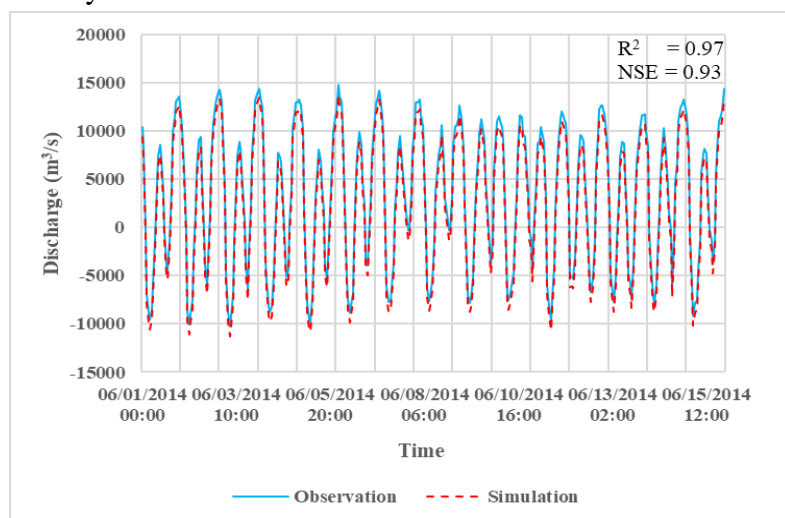


Figure 10. The calibration results of the discharge between the measured and calculated data from June 1, 2014, to June 15, 2014.

short section where flow is well-conserved, which contributes to the good flow calibration results (Figures 10–11).

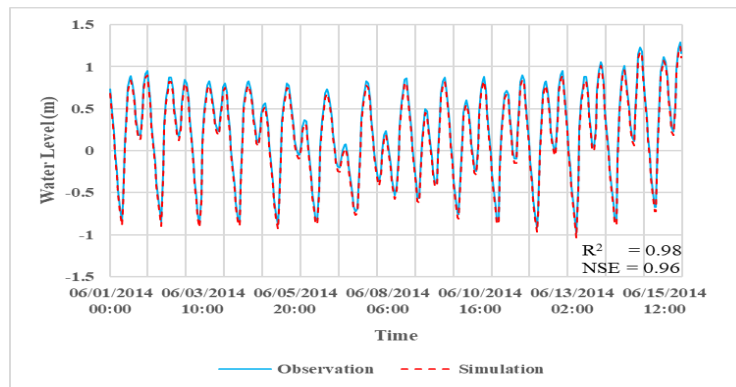


Figure 11. The calibration results of the water level between the measured and calculated data from June 1, 2014, to June 15, 2014.

To validate the hydraulic model, the calibrated parameter set mentioned above is used, and the calculation time is adjusted. The validation period is from 10:00 on June 6, 2018, to 10:00 on June 13, 2018. The water level and discharge data measured at the ST5 measurement stations during the supplementary survey are utilized (Refer to the location of ST5 in Figure 1).

The computed NSE and R^2 values at ST5 for water level are 0.9 and 0.89, respectively, while for discharge, they are 0.89 and 0.85. The comparison results at ST5 from June 6, 2018, to June 13, 2018, are presented in Figures 12-13.

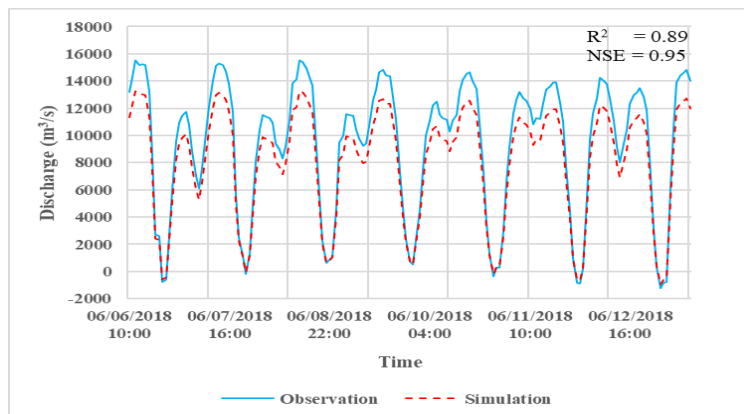


Figure 12. The comparison results between the measured and computed discharge at station ST5 from June 6, 2018, to June 13, 2018.

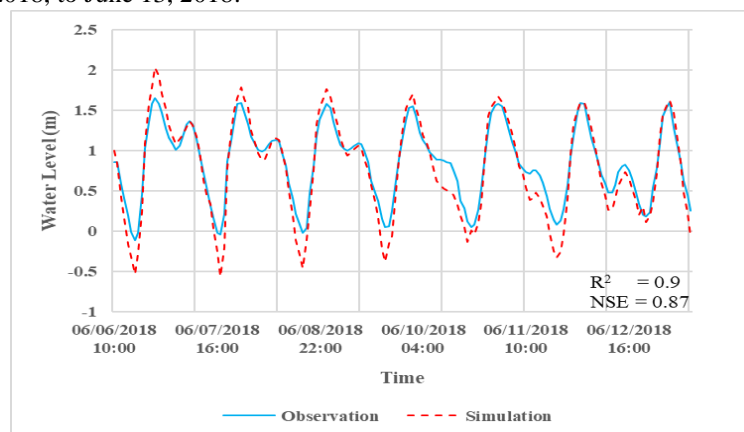


Figure 13. The comparison results between the measured and computed water level at station ST5 from June 6, 2018, to June 13, 2018.

Calibration and validation of the sediment transport model

The sediment deposition calibration process was carried out in June 2014. The results showed that the NSE and R^2 values for sediment deposition calibration were 0.74 and 0.89, respectively. Sediment concentration is a common parameter that is difficult to calibrate in sediment transport models, so the achieved calibration results can be considered quite good. The comparison between the calculated and measured sediment deposition for the calibration is presented in Figure 14.

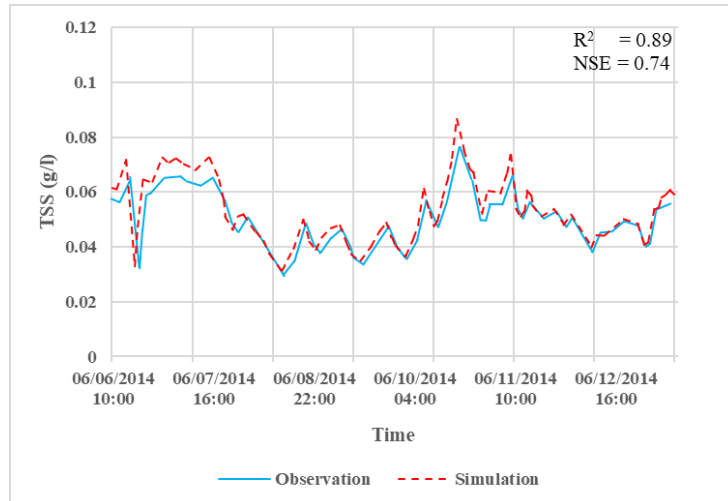


Figure 14. The calibrated results of suspended sediment between measurements and calculations from June 1, 2014, to June 15, 2014.

The parameter sets for the sediment transport model are extracted as shown in Table 3.

Table 3. The parameters in the sediment transport model.

Parameter	Value
Time step (Δt)	2 s
The mean diameter of particles. (D)	0.01 mm
The diameter of particles 90% (D_{90})	0.04 mm
Density (ρ_s)	2600 kg/m ³
Dynamic viscosity coefficient (ν)	1.01x10 ⁻⁶ m ² /s

The maps of the critical stresses of erosion (τ_e) and the critical stresses of deposition (τ_d) in the HYDIST-GPUs model were tested against the Sa Dec region and range from 0.2–0.35 N/m² (τ_e) and 0.03–0.06 N/m² (τ_d) (Figure 15).

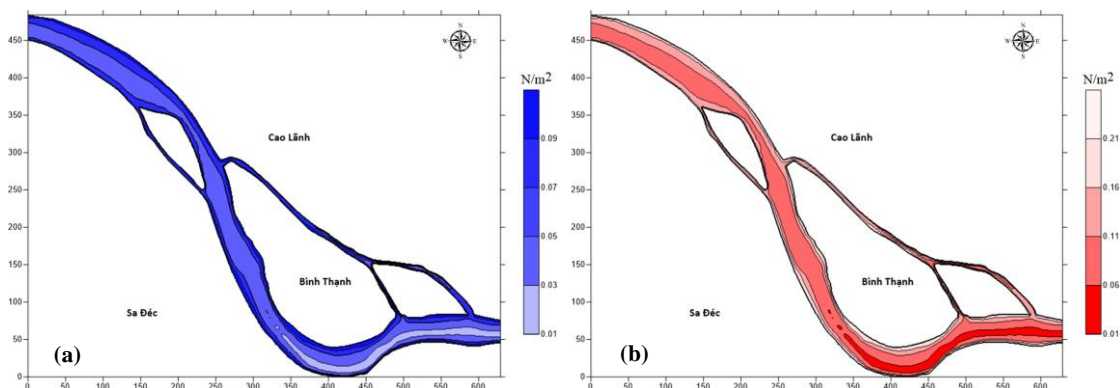


Figure 15. The maps: (a) The critical stresses of deposition τ_d ; (b) The critical stresses of erosion τ_e in the Sa Dec region.

The model validation for sediment transport is conducted from 10:00 on June 6, 2018, to 10:00 on June 13, 2018, based on the suspended sediment concentration at the ST5.

After obtaining the characteristic parameters for the sediment transport model for the entire computational domain, sediment transport calculations are performed until 2018. Subsequently, the computed suspended sediment concentration results from 10:00 on June 6, 2018, to 10:00 on June 13, 2018, at station ST5 are compared with the measured data. The NSE and R^2 values obtained during the validation process are quite good (0.74 for NSE and 0.89 for R^2). The comparison results between the computed and measured sediment transport are presented in Figure 16.

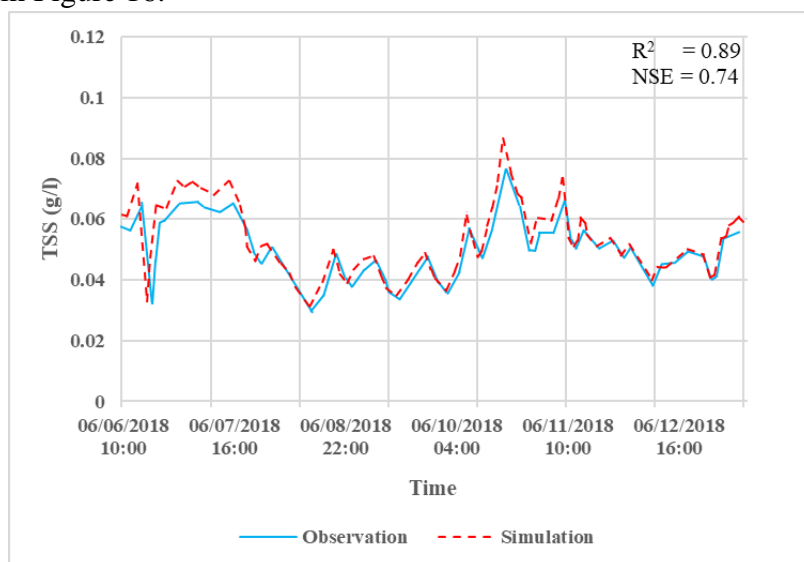


Figure 16. The validation results of sediment transport between the measured and computed data from June 6, 2018, to June 13, 2018.

3.2.4. Calculation of bank failure

The simulation of the bank failure rate of the section of the Tien River flowing through Sa Dec was carried out in 2015 and 2017. The parameter set of the model was established as shown in Table 4.

According to the theory of bank erosion, bank failure is expected to occur when FS value is less than 1. However, based on a study conducted by [45], it was observed that bank erosion starts to happen when the FS value is greater than 1.119. Therefore, for the specific case of Sa Dec, the calculations for bank erosion will consider FS values below 1.119 as indicative of bank erosion occurrence.

Table 4. The parameters of the model for bank erosion in Sa Dec.

Parameter		Value
Parameter settings	Critical FS	1.119
	The maximum distance between 2 points on a cross section (m)	0.23
	The number of points on a calculated cross section	100
	The number of sections for the calculated segment	65
	Tolerance	0.19
Soil parameters	fx Function	sin()
	The effective cohesion c (kN/m ²)	32
	The effective angle of friction ϕ (degree)	30
	Specific gravity of soil γ (kN/m ³)	19

	Parameter	Value
Simulation	The pore-water pressure u (kPa)	15
parameters	The horizontal seismic load kW (kN/m)	15

The simulation results from the bank erosion model in Sa Dec also include: the distribution of the safety factor FS and the width of the corresponding crack width BW for each longitudinal cross section along the riverbank. The bank erosion results are only calculated for the curved section of the riverbank on the side of Sa Dec city, with 65 cross sections as described in Figure 16.

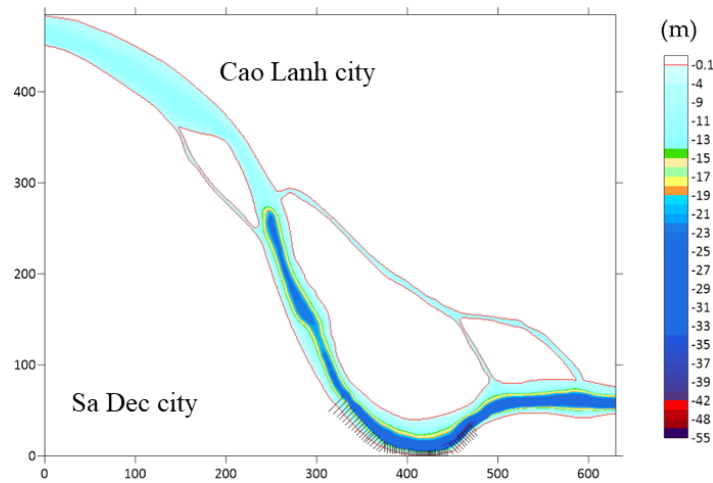


Figure 16. The cross-section of Tien River flowing Sa Dec City.

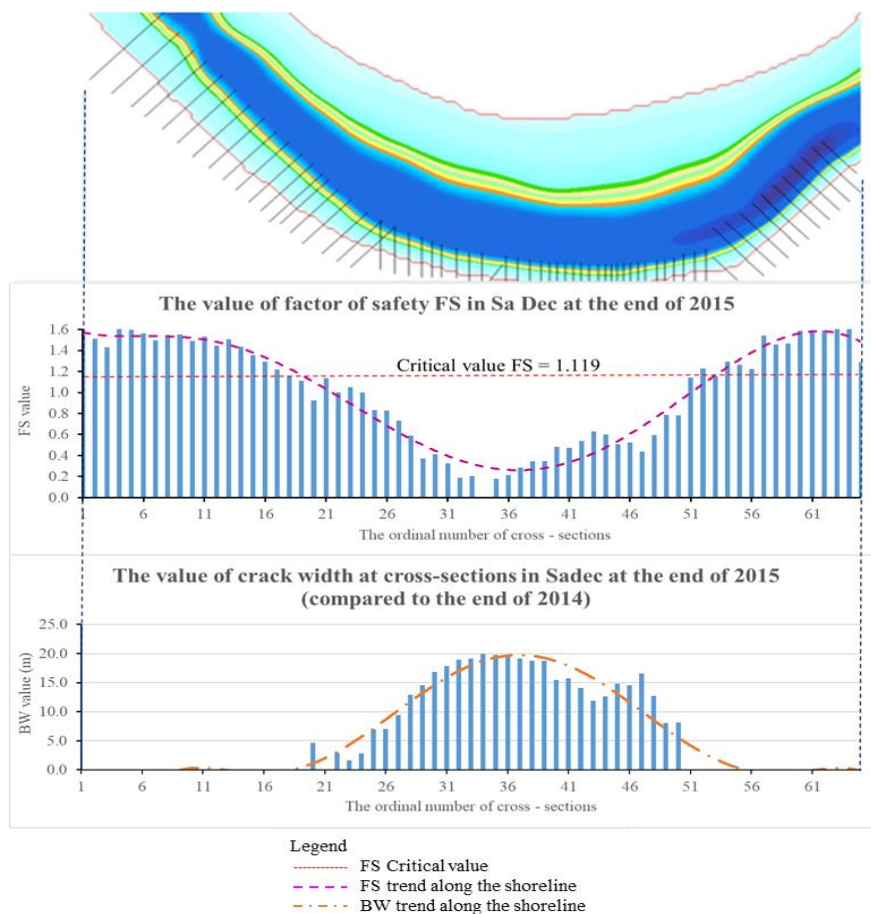


Figure 17. Simulation results of FS and BW coefficients along the riverbank of Sa Dec section in 2015.

The calculation results in 2015 showed that: in the curved section from cross section 19 to cross section 51, the result of $FS = 0.18 \div 1.11$ was less than the limit safety factor (limit $FS = 1.119$) (Figure 17). The sections before and after the curved section were more stable (with FS greater than the limit FS), with calculated FS ranging from 1.12 to 1.58 (Figure 17). In this section, although 7 rock revetments had been built (with a distance of about 50m between two revetments), the erosion process still occurred between two revetments.

The trend of variation of FS and BW along the curved section were also opposite to each other (Figure 18), at cross section 34 (the most curved section of the river), the BW in 2015 reached a value of 20m corresponding to a very low value of FS . Some selected cross sections (26, 34, and 44) in Figure 18 were extracted for further analysis.

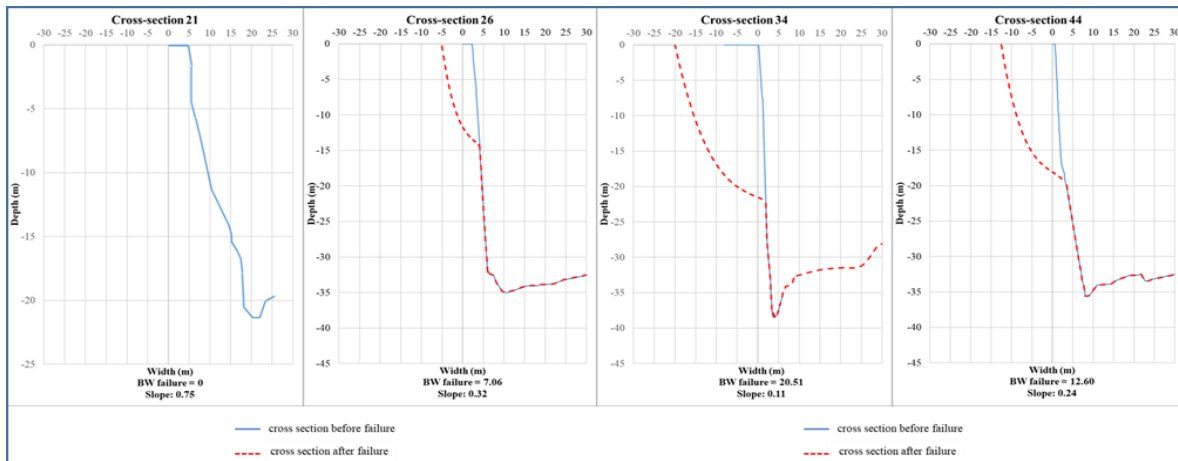


Figure 18. The results of bank erosion at sections 21, 26, 34 and 44 in 2015.

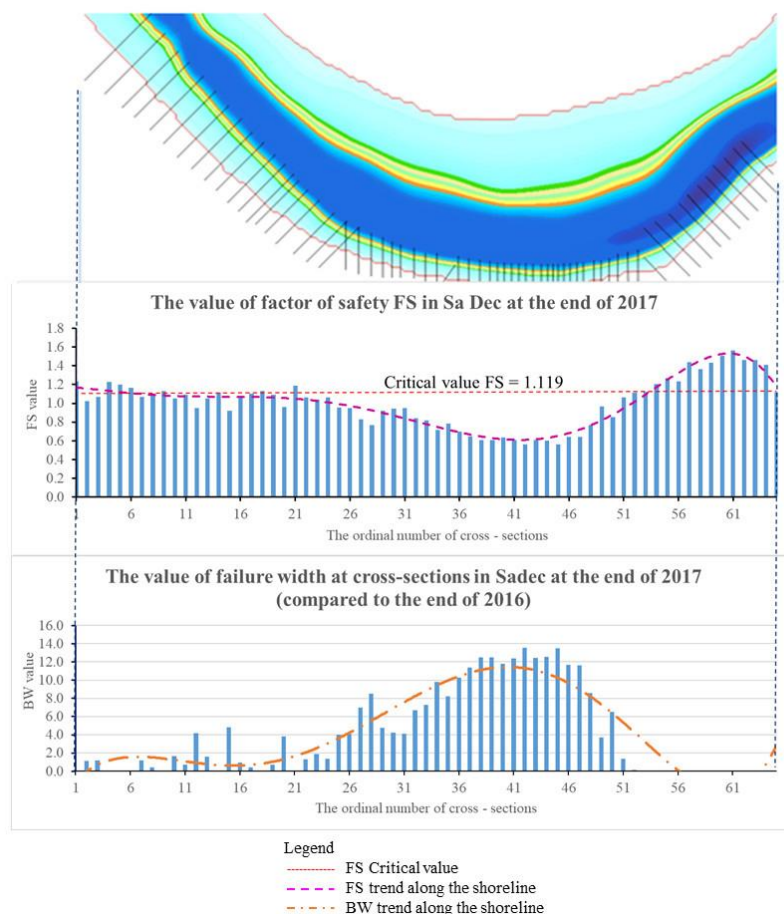


Figure 19. The results of FS and BW coefficients along the riverbank of Sa Dec section in 2017.

By 2017, the riverbank on the Sa Dec side showed a relatively similar trend to that of 2015, with intermittent erosion. The sections after the curved section exhibited higher stability, with FS values exceeding the critical FS. The calculated FS values in these sections ranged from 1.12 to 1.56. However, the sections before the curved section was less stable, as indicated by the FS. Both the FS values before the curved section and in the curved section are less than 1.119. Figure 19 presents the calculation results of FS and BW along the Sa Dec riverbank in 2017. The results indicated that the riverbanks are less stable. Specifically, the section in communes 3,4 Sa Dec (the sections before the curved section) had an FS value lower than 1.119, indicating a high risk of bank failure. The calculation results for the BW at cross-section 26 was approximately 4.14 m, at cross-section 34 was 9.78 m, and at cross-section 44 was 12.6 m (Figure 20).

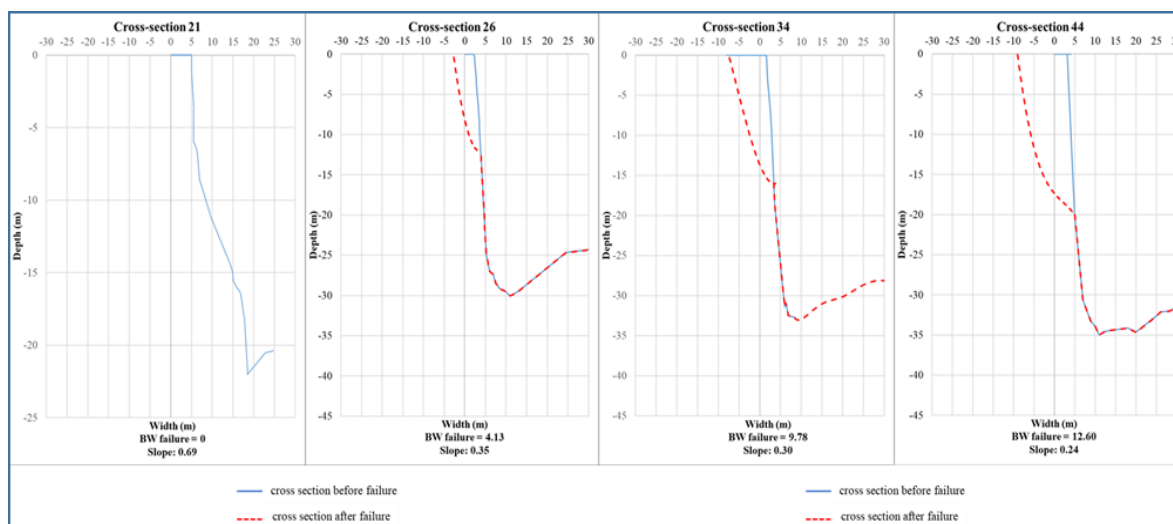


Figure 20. The results of bank erosion at sections 21 and 26 (a) 34 and 44 (b) in 2017.

4. Discussions

The statistics of the slope coefficient and crack width of the cross sections in the two calculation years are presented in Table 5.

Table 5. Statistics of slope coefficient and crack width of cross sections in 2015 and 2017 at some cross-sections (21, 26, 34 and 44).

Cross-sections	21		26		34		44	
Years	2015	2017	2015	2017	2015	2017	2015	2017
Slopes	0.75	0.69	0.32	0.35	0.115	0.3	0.24	0.24
Failure Width (BW m)	0	0	7.1	4.14	20.5	9.78	12.6	12.6

According to the calculation results, it is observed that the potential for bank failure occurs before and in the curved arc sections. The high potential for bank failure occurred between cross-section 34 and cross-section 44, with corresponding BW of 15.5 m and 12.6 m in 2015. By 2017, the BW at these two cross-sections corresponded to 9.78 m and 12.6 m.

The calculated BW at cross-sections 21, 26, 34, and 44 in 2017 was lower than in 2015. At cross-section 26, the bank erosion potential in 2015 was 7.1 m, but by 2017, it decreased to 4.14 m. However, the cross-sections before the curved section show significantly greater signs of instability compared to 2015. These calculated results align well with the forecasted results from the study by Dinh Cong San for commune 3,4, Sa Dec (erosion ranging from 5–8 m) [46].

The Sa Dec riverbank started to erode when the slope of the bank was relatively steep (the slope coefficient of the bank was quite small) as recorded in Table 5, where cross-section 21 was not eroded (FS coefficient here was about 1.11, and the maximum slope coefficient of the bank was accepted at 0.69. Compared to the bank slope coefficient in Tan Chau, the maximum slope of the bank here was steeper. This is also consistent with reality because the cohesion force of the soil in Sa Dec (32 kN/m^2) is larger than that in Tan Chau (24 kN/m^2). In the Sa Dec bank survey, it was found that the vegetation cover was more extensive than on the An Giang bank opposite to Chinh Sach islet. In the model, the cohesion factor of the soil due to plant roots was also included in the cohesion force. The results from the HYDIST-GPUs-RF model for the Tien River section flowing through Sa Dec City indicate that the section with the most significant erosion is located in An Hiep Commune [28]. This is relatively accurate compared to the result obtained from the calculation of the bank line change using remote sensing [6]. The maximum distance between the bank line before and after 10 years (2009–2019) is 279 meters [47].

5. Conclusions

The simulations from the HYDIST-GPUs-RF model are quite consistent with those from the GEOSLOPE software. Slope stability calculations are very detailed and carried out for each cross-section. To save time and effort, the slope calculation is not performed for the entire length of the riverbank. Based on the calculation results of the dynamic hydraulic model, each small section of the bank that is at risk of erosion (i.e. those sections with significant depth loss based on the calculation) will be identified, and only those sections will be included in the HYDIST-GPUs-RF model for slope simulation and then the bathymetry will be updated. However, currently, the sections are not automatically cut. These limitations are expected to be addressed and improved in future developments.

The model was tested on some sections of the Tien River passing through Tan Chau Town in An Giang Province and Sa Dec City. The results of the simulated river morphology in different years are quite consistent with the actual morphology of the area (based on the comparison with remote sensing analysis and observations). The results show that for the geological structure of this section of the Tien River, the stability level of the bank corresponded to a limit factor of safety of 1.119. The model is not only applicable for calculating river morphology in the Mekong Delta region but can also be used to calculate the morphology and erosion of any other river section in Vietnam. However, the parameters in the model need to be adjusted to fit each region. The calculation results also depend heavily on the reliability of the input data. Therefore, to successfully apply the HYDIST-GPUs model in calculating river morphology, the first important step is to conduct a thorough survey, collect long-term (multi-year) and supplementary measurement data for the region.

Author Contributions: Conceptualization, T.T.K., N.T.B.; methodology, T.T.K., P.A.T., N.T.B., N.K.P.; software, T.T.K., N.D.Q.H., P.T.M.D., P.A.T.; validation, P.T.M.D.; formal analysis, T.T.K., P.T.M.D., N.D.Q.H.; investigation, N.T.B., N.K.P.; resources, N.T.B.; data curation, N.D.Q.H., N.T.B.; writing—original draft preparation, T.T.K., N.T.B.; writing—review and editing, T.T.K., N.T.B.; visualization, P.A.T., N.D.Q.H.; supervision, N.K.P., N.T.B.; project administration, N.K.P.; funding acquisition, N.K.P.

Funding: We would like to thank Ho Chi Minh City University of Technology (HCMUT), VNU-HCM, for the support of time and facilities for this study.

Conflicts of Interest: The authors declare no conflict of interest.

References

1. Agnihotri, A.K.; Ohri, A.; Mishra, S. Channel planform dynamics of lower Ramganga River, Ganga basin, GIS and remote sensing analyses. *Geocarto Int.* **2020**, *35*(9), 934–953.

2. Church, M.; Ferguson, R. Morphodynamics: Rivers beyond steady state. *Water Resour. Res.* **2015**, *51*(4), 1883–1897.
3. Das, T.K.; Haldar, S.K.; Gupta, I.D.; Sen, S. River bank erosion induced human displacement and its consequences. *Living Rev. Landscape Res.* **2014**, *8*(3), 1–35.
4. Duc, N.A.; Nguyen, L.T.; Thai, T.H.; Khan, A.; Rautenstrauch, K.; Schmidt, C. Assessing cumulative impacts of the proposed Lower Mekong Basin hydropower cascade on the Mekong River floodplains and Delta—Overview of integrated modeling methods and results. *J. Hydrol.* **2020**, *581*, 122511.
5. Hasanuzzaman, M.; Gayen, A.; Shit, P.K. Channel dynamics and geomorphological adjustments of Kaljani River in Himalayan foothills. *Geocarto Int.* **2022**, *37*(16), 4687–4713.
6. Khoi, D.N.; Dang, T.D.; Pham, L.T.; Loi, P.T.; Thuy, N.T.D.; Phung, N.K.; Bay, N.T. Morphological change assessment from intertidal to river-dominated zones using multiple-satellite imagery: A case study of the Vietnamese Mekong Delta. *Reg. Stud. Mar. Sci.* **2020**, *34*, 101087.
7. Kondolf, G.M.; Schmitt, R.J.; Carling, P.; Darby, S.; Arias, M.; Bizzi, S.; Castelletti, A.; Cochrane, T.A.; Gibson, S.; Kumm, M.; Oeuring, C.; Rubin, Z.; Wild, T. Changing sediment budget of the Mekong: Cumulative threats and management strategies for a large river basin. *Sci. Total. Environ.* **2018**, *625*, 114–134.
8. Tran, D.D.; van Halsema, G.; Hellegers, P.J.; Hoang, L.P.; Ludwig, F. Long-term sustainability of the Vietnamese Mekong Delta in question: An economic assessment of water management alternatives. *Agric. Water. Manage.* **2019**, *223*, 105703.
9. Van, B.D.; Kantoush, S.; Sumi, T. Changes to long-term discharge and sediment loads in the Vietnamese Mekong Delta caused by upstream dams. *Geomorphology* **2020**, *353*, 107011.
10. Lane, S.N.; Richards, K.S. Linking river channel form and process: time, space and causality revisited. *Earth Surf. Processes Landforms* **1997**, *22*(3), 249–260.
11. Lawler, D. The importance of high-resolution monitoring in erosion and deposition dynamics studies: examples from estuarine and fluvial systems. *Geomorphology* **2005**, *64*(1–2), 1–23.
12. Wu, B.; Zheng, S.; Thorne, C.R. A general framework for using the rate law to simulate morphological response to disturbance in the fluvial system. *Prog. Phys. Geogr.* **2012**, *36*(5), 575–597.
13. Grant, G.E. (Eds) The geomorphic response of gravel-bed rivers to dams: perspectives and prospects. *Gravel-bed Rivers: Processes, tools, environments*. Wiley Online Library, **2012**, 165–181.
14. Van, M.N.; Dung, N.V.; Hung, N.N.; Kumm, M.; Merz, B.; Apel, H. Future sediment dynamics in the Mekong Delta floodplains: Impacts of hydropower development, climate change and sea level rise. *Global Planet Change* **2015**, *127*, 22–33.
15. Fryirs, K.A. River sensitivity: a lost foundation concept in fluvial geomorphology. *Earth Surf. Processes Landforms* **2017**, *42*(1), 55–70.
16. Fryirs, K.A.; Brierley, G.J. *Geomorphic analysis of river systems: an approach to reading the landscape*: John Wiley & Sons, 2012.
17. Briggs, K.B. *High-frequency acoustic scattering from sediment interface roughness and volume inhomogeneities*: University of Miami, 1994.
18. <https://www.mikepoweredbydhi.com/>.
19. <https://www.tudelft.nl/en/>.
20. Galland, J.C.; Goutal, N.; Hervouet, J.M. TELEMAC: A new numerical model for solving shallow water equations. *Adv. Water Resour.* **1991**, *14*(3), 138–148.

21. Gad, M.A.; Saad, A.; El-Fiky, A.; Khaled, M. Hydrodynamic modeling of sedimentation in the navigation channel of Damietta Harbor in Egypt. *Coastal Eng. J.* **2013**, *55*(2), 350007-1-1350007-31.
22. Zhang, Y. CCHE2D-GUI-graphical user interface for the CCHE2D model user's manual-version 2.2. 2005.
23. Van, Rijn, L.C.; van Rossum, H.; Termes, P. Field verification of 2-D and 3-D suspended-sediment models. *ISH J. Hydraul Eng.* **1990**, *116*(10), 1270-1288.
24. Chang, H.H. Case study of fluvial modeling of river responses to dam removal. *J Hydraul Eng.* **2008**, *134*(3), 295-302.
25. Lee, H.Y.; Hsieh, H.M.; Yang, J.C.; Yang, C.T. Quasi-two-dimensional simulation of scour and deposition in alluvial channels. *J. Hydraul. Eng.* **1997**, *123*(7), 600-609.
26. Le, G.S.; Ho, L.H.; Tran, L.T.; Park, E. F28: A Novel Coupling Strategy for 1D-2D Hydraulic Models for Flood Risk Assessment of the Mekong Delta. Available at SSRN 4358313. 2023, pp. 23.
27. Giang, N.; Izumi, N. (Eds) Application of an integrated morphological model to Red River network. 2nd IAHR Symposium on River, Coastal and Estuarine Morphodynamics, RCEM 2001, 2001.
28. Kim, T.T.; Huong, N.T.M.; Huy, N.D.Q.; Tai, P.A.; Hong, S.; Quan, T.M.; et al. Assessment of the impact of sand mining on bottom morphology in the Mekong River in an Giang Province, Vietnam, using a hydro-morphological model with GPU computing. *Water* **2020**, *12*(10), 2912.
29. Cole, R.A.; Wu, Q. (Eds) Predicting bank failures using a simple dynamic hazard model. 22nd Australasian Finance and Banking Conference, Citeseer, 2009.
30. Rinaldi, M.; Darby, S.E. Modelling river-bank-erosion processes and mass failure mechanisms: progress towards fully coupled simulations. *Earth Surf. Processes* **2007**, *11*, 213-239.
31. Duong, T.T.; Do, M.D. Riverbank stability assessment under river water level changes and hydraulic erosion. *Water* **2019**, *11*(12), 2598.
32. Abderrezzak, K.E.K.; Moran, A.D.; Tassi, P.; Ata, R.; Hervouet, J.M. Modelling river bank erosion using a 2D depth-averaged numerical model of flow and non-cohesive, non-uniform sediment transport. *Adv. Water Resour.* **2016**, *93*, 75-88.
33. Cribb, M.; Darby, S. (Eds) Modelling the Influence of Riparian Vegetation on River Bank Erosion. AGU Fall Meeting Abstracts, 2002.
34. Dahale, P.; Nalgire, T.; Mehta, A.; Hiwase P. Slope stability analysis by GeoSlope. *Triple Helix* **2020**, *10*(01), 71-75.
35. Van Rijn, L.C. Principles of sediment transport in rivers, estuaries and coastal seas 1993.
36. Mishal, U.R.; Khayyun, T.S. Stability analysis of an earth dam using GEO-SLOPE model under different soil conditions. *Eng. Tech. J.* **2018**, *36*(5), 523-532.
37. Arshad, I.; Babar, M.M. Finite element analysis of seepage through an earthen dam by using geo-slope (SEEP/W) software. *Int. J. Res.* **2014**, *1*(8), 616-634.
38. Watson, A.; Basher, L. Stream bank erosion: a review of processes of bank failure, measurement and assessment techniques, and modelling approaches. A report prepared for stakeholders of the Motueka Integrated Catchment Management Programme the Raglan Fine Sediment Study Landcare Research, Hamilton, New Zealand. 2006.
39. Xu, N.; Xia, W.; Zhao, B.; Wu, T. Eds. The improved Simplified Bishop's Method considering the Difference of Inter-slice Shearing Force. Hydraulic Engineering III: Proceedings of the 3rd Technical Conference on Hydraulic Engineering (CHE 2014), Hong Kong, 13-14 December 2014, CRC Press, 2014.

40. Bishop, A.W. The use of the slip circle in the stability analysis of slopes. *Geotechnique* **1955**, *5(1)*, 7–17.
41. Janbu, N. Editor Application of composite slip surface for stability analysis. European Conference on Stability of Earth Slopes Stockholm, Sweden, 1954.
42. Agam, M.; Hashim, M.; Murad, M.; Zabidi, H. (Eds) Slope sensitivity analysis using spencer's method in comparison with general limit equilibrium method. *Procedia Chem.* **2016**, *19*, 651–658.
43. Van, T.N. Editor Coastal erosion, river bank erosion and landslides in the Mekong Delta: Causes, effects and solutions. Geotechnics for Sustainable Infrastructure Development, Springer, 2020.
44. Nguyen, N.A. Why does the river erosion situation become more complicated in the Mekong delta? *VN J. Sci. Technol. Eng.* **2018**, *60(1)*, 73–82.
45. Hung, L.M.; San, D.C. Bank erosion Mekong River. Southern Institute for Water Resources, 2002.
46. Hung, L.M.; Tanaka, H.; Tu, N.T.; Viet, N.T. (Eds) Prediction of river bank erosion in the Lower Mekong River Delta. Vietnam – Japan Estuary Workshop, Hanoi, Vietnam, 2006.
47. Kim, T.T.; Diem, P.T.M.; Trinh, N.N.; Phung, N.K.; Bay, N.T. Riverbank movement of the Mekong River in An Giang and Dong Thap Provinces, Vietnam in the period of 2005–2019. *VN J. Hydrometeorol.* **2020**, *6*, 35–45.